AJNR

Hemodynamic Changes in Patients with Arteriovenous Malformations Assessed Using High-Resolution 3D Radial Phase-Contrast MR Angiography

W. Chang, M.W. Loecher, Y. Wu, D.B. Niemann, B. Ciske, B. Aagaard-Kienitz, S. Kecskemeti, K.M. Johnson, O. Wieben, C. Mistretta and P. Turski

AJNR Am J Neuroradiol 2012, 33 (8) 1565-1572
doi: https://doi.org/10.3174/ajnr.A3010
http://www.ajnr.org/content/33/8/1565

ORIGINAL RESEARCH

Hemodynamic Changes in Patients with Arteriovenous Malformations Assessed Using High-Resolution 3D Radial Phase-Contrast MR Angiography

W. Chang
M.W. Loecher
Y. Wu
D.B. Niemann
B. Ciske
B. Aagaard-Kienitz
S. Kecskemeti
K.M. Johnson
O. Wieben
C. Mistretta
P. Turski

BACKGROUND AND PURPOSE: Arteriovenous malformations have a high lifetime risk of hemorrhage; however, treatment carries a significant risk of morbidity and mortality, including permanent neurologic sequelae. WSS and other hemodynamic parameters are altered in patients with symptomatic AVMs, and analysis of hemodynamics may have value in stratifying patients into different risk groups. In this study, we examined hemodynamic data from patients with stable symptoms and those who presented with acute symptoms to identify trends which may help in risk stratification.

MATERIALS AND METHODS: Phase-contrast MRA using a radial readout (PC-VIPR) is a fast, high-resolution technique that can acquire whole-brain velocity-encoded angiograms with scan times of approximately 5 minutes. Ten patients with AVMs were scanned using PC-VIPR; velocity, area, flow, and WSS in vessels feeding the AVMs and normal contralateral vessels were calculated using velocity data from the phase-contrast acquisition.

RESULTS: Patients with an asymptomatic presentation or mild symptoms ($n = 4$) had no significant difference in WSS in feeding vessels compared with normal contralateral vessels, whereas patients presenting with hemorrhage, severe headaches/seizures, or focal neurologic deficits ($n = 6$) had significantly higher WSS in feeding vessels compared with contralateral vessels.

CONCLUSIONS: In this study, we demonstrate that estimates of WSS and other hemodynamic parameters can be obtained noninvasively in patients with AVMs in clinically useful imaging times. Variation in WSS between feeders and normal vessels appears to relate to the clinical presentation of the patient. Further analysis of hemodynamic changes may improve characterization and staging of AVM patients, when combined with existing risk factors.

ABBREVIATIONS: CFD = computational fluid dynamics; ICH = intracranial hemorrhage; PC-MRA = phase-contrast MRA; PC-VIPR = phase-contrast vastly undersampled projection reconstruction; VEGF = vascular endothelial growth factor; WSS = wall shear stress

Untreated AVMs present a clinical dilemma because they carry a significant annual risk of intracranial hemorrhage, with associated morbidity and mortality, but current treatment options also carry significant risks. Prognostic information on the risk of rupture of individual AVMs may allow patients who would benefit from definitive treatment to be differentiated from those who can be managed conservatively. In this report, we describe a noninvasive technique for characterizing WSS and other hemodynamic parameters in patients with arteriovenous malformations, and relate these data to the patients' clinical presentation.

AVMs carry a significant risk of hemorrhage, with a 1%–33% annual risk of bleeding and a 40%–70% lifetime risk.[1-3] Hemorrhage has high morbidity and mortality, with a 5%–25% chance of death within 1 year and a 25%–40% risk of permanent neurologic deficits.[3-5] A 24-year longitudinal study of symptomatic patients who declined treatment reported a 4% chance of hemorrhage on an annual basis. The authors found that 40% of patients had hemorrhage during the study period and 23% of the patients died from the sequelae of ICH.[6] Currently, the risks of both hemorrhage and treatment are assessed based on anatomic features of AVMs and the patient's presentation and clinical course. Reports from multiple investigators consistently focus on 4 main risk factors for intracranial hemorrhage: deep brain location, deep venous drainage, initial presentation with hemorrhage, and associated aneurysms, with 1 report finding that patients with all 4 risk factors have as high as a 33% annual risk of hemorrhage.[1-3]

Hemodynamic parameters such as pressure and WSS are well known to cause vascular remodeling and may have value in assessing the risk of hemorrhage. WSS can be measured by multiplying the derivative of blood velocity at the vessel wall by the viscosity of blood in the vessel, and has been show to be altered in AVMs, due to derangements in flow physiology and endothelial changes. Several studies have reported that high WSS and circumferential strain in AVM feeders induce endothelial changes, resulting in expression of intracellular factors such as matrix metalloprotease 9, platelet-drived growth fac-

Received July 2, 2011; accepted after revision October 31.

From the Departments of Medical Physics (W.C., M.W.L., Y.W., S.K., K.M.J., O.W., C.M.), Radiology (W.C., B.C., C.M., P.T.), and Neurosurgery (D.B.N., B.A.-K.), University of Wisconsin, Madison, Wisconsin and University of Wisconsin School of Medicine and Public Health (B.C.), Madison, Wisconsin.

Research supported by NIH R21 EB00944.

Please address correspondence to Warren Chang, Department of Radiology, University of Wisconsin, Madison, Wisconsin Institutes for Medical Research, 1111 Highland Ave, Rm 1316, Madison, WI 53705; e-mail: wmchang2@wisc.edu

http://dx.doi.org/10.3174/ajnr.A3010

tor, tyrosine kinase with immunoglobin-like and endothelial growth factor like domains, and VEGF that promote vessel remodeling.[7-13] In mouse models of hereditary hemorrhagic telangiectasia with activin receptor-like kinase deficiencies, researchers have found that increased WSS induces increased synthesis of VEGF, leading to enlarged and dilated vessels in the mouse brain, with vascular morphology similar to AVMs in humans.[12,13]

WSS can be estimated from velocity measurements from PC-MRA, Doppler sonography, and CFD. PC-MRA and automated spline interpolation can be used to estimate WSS, but a limitation of prior investigations of WSS using MRA is the lack of sufficient spatial resolution and coverage necessary to visualize the boundary zone and vessels of interest within clinically useful scan times.[14] When imaging AVMs, a large field of view that encompasses the entire brain is required to visualize both arterial and venous components. Whole-brain coverage also allows comparison of flow conditions in AVM-feeding arteries with those in normal contralateral vessels. We have implemented a highly accelerated 3D radial phase-contrast MRA technique, called PC-VIPR, capable of acquiring high-resolution PC angiograms of the whole brain with velocity information.[15-17] In this study, we use the velocity data from PC-VIPR to estimate WSS and other hemodynamic parameters in 2 groups of patients and relate their hemodynamic profiles to their clinical presentations.

Materials and Methods

Patient Selection

The imaging studies were performed in compliance with Health Insurance Portability and Accountability Act regulations and using a protocol approved by the local institutional review board. Ten patients presenting with AVMs were imaged using PC-VIPR. Patients were divided into 2 groups. Group 1 ($n = 4$; 2 men, 2 women; ages 33–56, mean age 42 years) included patients who were asymptomatic with the AVM detected as an incidental finding, or patients who had headaches/seizures that were clinically stable and medically managed. All 4 patients had Spetzler-Martin grade 3 AVMs, with an average size of 3.25 cm. Group 2 ($n = 6$; 1 man, 5 women; ages 20–47, mean age 37.8 years) included patients who presented with hemorrhage, focal neurologic deficits, or severe or uncontrollable headaches/seizures, who received treatment by surgical resection, radiosurgery, embolization, or combination therapy after the scans were completed. Spetzler-Martin grades of these 6 AVMs ranged from 1–4 (average 2.83), and average size was 2.75 cm. A total of 42 vessels were assessed in group 1, and 58 were assessed in group 2.

MR Protocol

Patients were scanned using a clinical 3T MR system (HD 750; GE Healthcare, Milwaukee, Wisconsin) with an 8-channel head coil (Excite HD Brain Coil, GE Healthcare). Immediately after clinical imaging, the 3D radial PC-VIPR scan was acquired (scan parameters were TR/TE = 8.2/2.8, $\alpha = 20$, bandwidth = 83.3 KHz, scan time = 300 seconds, velocity encoding = 80 cm/s, field of view = $220 \times 220 \times 220$ mm^3, resolution = $0.67 \times 0.67 \times 0.67$ mm^3). Velocity data from the PC-VIPR examinations were used for hemodynamic evaluation.[16,17]

Postprocessing/Cut-Plane Placement

The vessels of interest were semiautomatically extracted from the imaging volume using commercially available segmentation software (Mimics; Materialise US, Plymouth, Michigan). After segmentation, the velocity data from the PC-VIPR scans were imported into a commercial software product that is designed to measure flow parameters (Ensight; Computational Engineering International, Apex, North Carolina). Cut-planes were then placed in Ensight in the vessels of interest. AVMs were divided into anterior circulation, posterior circulation, or mixed, based on the vessels from which the blood supply was derived. For anterior AVMs, cut-planes were placed in the primary feeders of the AVM, as well as the M1 segment of each MCA and the distal segment of each terminal ICA. For posterior AVMs fed from the basilar artery and PCAs, cut-planes were placed in the primary feeders of the AVM, as well as the midbasilar artery and P1 segment of each posterior cerebral artery. For those posterior AVMs with feeders originating from the PICAs, cut-planes were also made in the vertebral arteries proximal to the PICA takeoff. For mixed AVMs, cut-planes were placed in both anterior and posterior vessels. Fig 1 shows images of cut-planes being placed in the feeder and the MCA/ICA of an anterior circulation AVM, and of points being selected around the MCA of the same patient.

WSS

After cut-plane placement, 2D planes were extracted for analysis in a custom Matlab (The MathWorks, Natick, Massachusetts) environment, which tabulated velocity, vessel diameter, WSS, and flow.[14,18,19] In this processing chain, vessel boundaries were manually segmented from magnitude images and the flow profile was interpolated using B-splines. Time-averaged flow and mean velocities were calculated directly from the B-spline fit. Average WSS was calculated utilizing the derivative of the interpolated velocity at the wall, averaged over the diameter and cardiac cycle. This 2D technique was used to generate all quantitative WSS and flow measurements in this report. A qualitative WSS measure was also determined by automatic 3D segmentation of the vessel boundary utilizing thresholding of the PC-MRA images. In 3D, second-order polynomials were used to fit the velocity at the wall. Whole-brain surface-rendered WSS maps were determined from the derivative of the second-order polynomial at the wall. These 3D maps were used to evaluate global differences and trends in WSS.[14] Fig 2*A*, -*B* show sagittal MR and digital subtraction angiograms of a left thalamic AVM, and Fig 2*C* shows a qualitative WSS map of the AVM generated using polynomial analysis, showing increased WSS in feeding vessels and in the arterialized draining vein.

Statistics

A 2-sample *t* test for independent samples was conducted to compare the mean WSS, velocity, flow, and vessel diameter of vessels feeding AVMs to normal contralateral vessels. A *P* value of .05 was considered statistically significant.

Results

Group 1 patients had an average WSS of 1.555 N/m^2 in ipsilateral vessels feeding the AVM and a WSS of 1.494 N/m^2 in normal contralateral vessels. A 2-sample *t* test found no significant difference between the 2 values, with a *P* value of .31. Group 2 patients had an average WSS of 1.607 N/m^2 in ipsilateral vessels feeding the AVM and a WSS of 1.146 N/m^2 in normal contralateral vessels. A 2-sample *t* test found a signif-

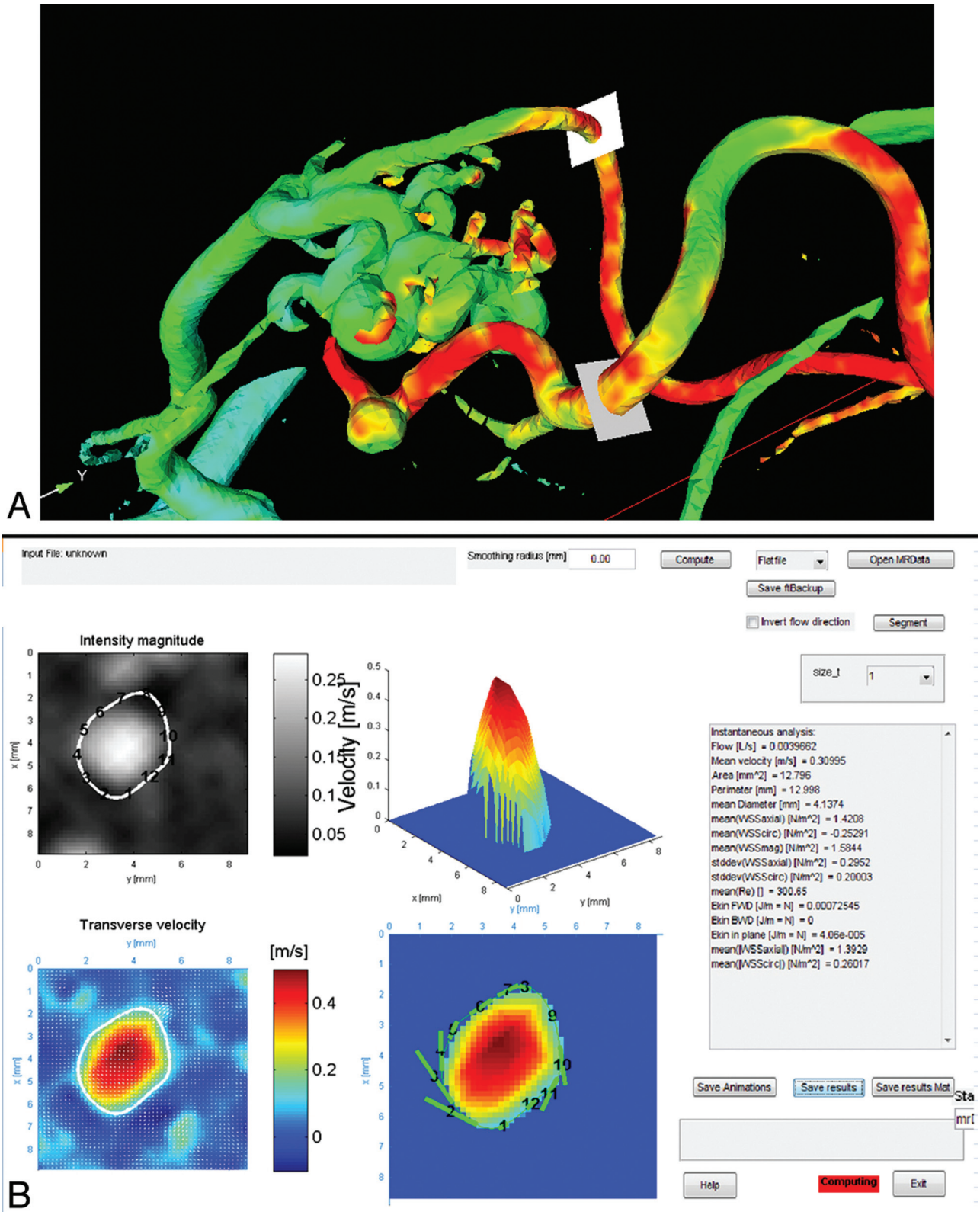

Fig 1. *A*, Cut-planes being placed in vessels feeding a right frontoparietal AVM. *B*, Points being selected around a vessel feeding the same AVM, and WSS being calculated in a custom Matlab environment.

icant difference between the 2 values, with a *P* value of .003. Group 1 patients had significantly larger average vessel diameter (4.57 mm compared with 3.66 mm) in vessels feeding the AVM compared with normal contralateral vessels ($P = .005$), while group 2 patients had a larger diameter as well (4.34 mm compared with 3.84 mm), but the difference was not statistically significant ($P = .11$).

Both group 1 and group 2 patients had increased mean

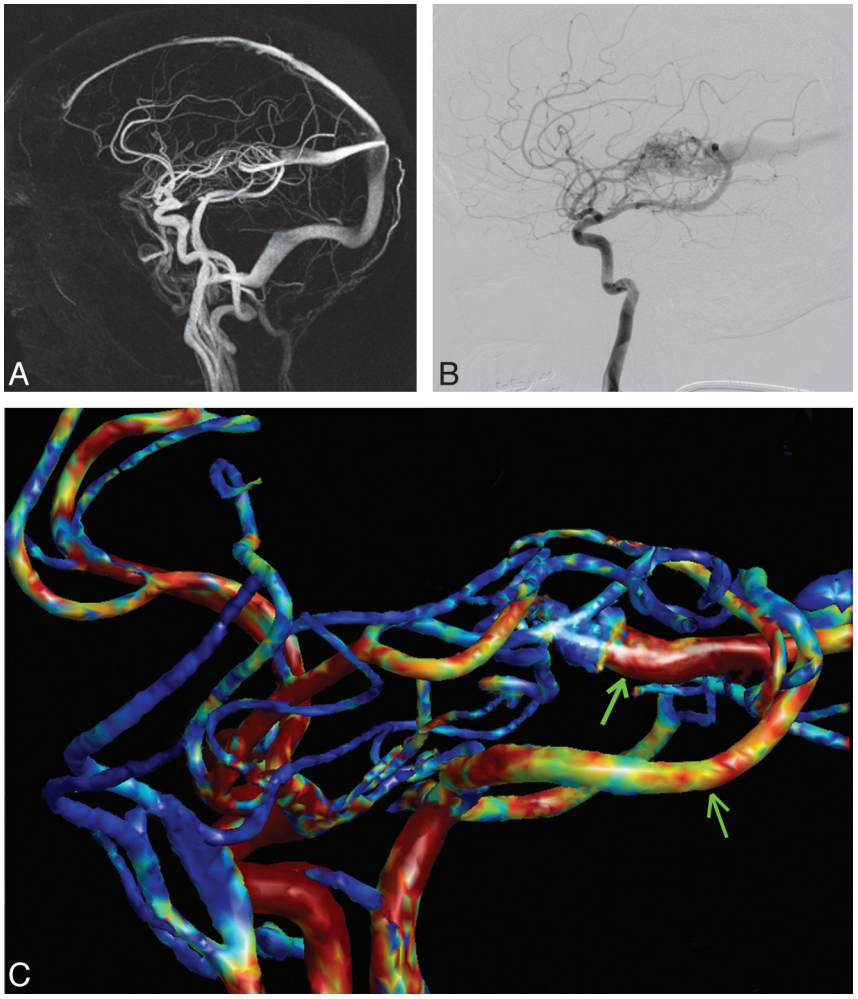

Fig 2. *A*, Sagittal maximum intensity projection of a complex difference image acquired using PC-VIPR, showing a left thalamic AVM, arterial feeders, and the AVM nidus. *B*, DSA angiogram of the same AVM for comparison, showing contrast flow through feeding vessels. *C*, WSS map of the AVM generated from velocity data from PC-VIPR, showing increased WSS in feeding vessels and in the arterialized draining vein (*arrows*).

Hemodynamics of Group 1 and Group 2 patients

	Axial WSS (N/m^2)	Diameter (mm)	Velocity (cm/s)	Flow (ml/s)
Group 1 (mild, stable symptoms)				
Ipsilateral vessels (n = 23)	1.555 (P = 0.31)	4.57[a] (P = 0.005)	41.3[a] (P = 0.001)	6.23[a] (P = 0.005)
Contralateral vessels (n = 19)	1.494	3.66	31.1	3.82
Group 2 (severe, acute symptoms)				
Ipsilateral vessels (n = 32)	1.607[a] (P = 0.003)	4.34 (P = 0.11)	41.7[a] (P = 0.009)	4.57[a] (P = 0.026)
Contralateral vessels (n = 26)	1.146	3.84	29.6	3.32

[a] Statistical significance, $P < .05$.

time-average velocity in ipsilateral feeding vessels compared with normal contralateral vessels (41.3 versus 31.1 in group 1; 41.7 versus 29.6 in group 2), and the difference was statistically significant in both cases ($P = .001$ and $P = .009$, respectively). Both group 1 and group 2 patients had increased flow in ipsilateral feeding vessels compared with normal contralateral vessels (6.23 versus 3.82 in group 1; 4.57 versus 3.32 in group 2), and the difference was, again, statistically significant in both cases ($P = .005$ and $P = .026$, respectively). The results are summarized in the Table.

An example of a group 1 patient is presented in Figs 3 and 4. Fig 3 summarizes this patient, who had a right temporal AVM fed from the anterior circulation and had clinically stable symptoms that have been medically managed since her diagnosis in 1990. Fig 3 shows hemodynamic data from this patient, showing similar WSS but increased flow, velocity, and vessel caliber. Fig 4*A* shows a coronal maximum intensity projection of a complex difference image acquired using PC-VIPR to establish the orientation of the AVM, and Fig 4*B* shows a velocity image of the whole brain. Note the increased diameter of the ICA/MCA on the right (ipsilateral to AVM) compared with the left side. Fig 4*C* shows a WSS map of the whole brain calculated from PC-VIPR velocity data, and Fig 4*D* shows a detailed velocity map of the circle of Willis. Note similar WSS in the MCA and ICA of right-sided vessels compared with the left side.

Group 1 Example:

56 y/o female patient with a 20 year history of seizures easily controlled by levetiracetam. Her only current symptoms are occasional mild headaches controlled with ibuprofen.

AVM Pathology: Right anterior temporal lobe AVM supplied by branches of the right middle cerebral artery (Spetzler-Martin Grade III).

The flow features in this patient are summarized below.

Artery	WSS (N/m^2)	Flow (ml/sec)	Velocity (cm/s)	Diameter (mm)
RICA	1.431	**8.19**	**39.7**	**5.46**
LICA	1.409	5.53	34.1	4.69
RMCA	1.675	**5.13**	**47.3**	**4.15**
LMCA	1.642	2.18	30.5	3.04
Main Feeder	1.456	**7.15**	**37.8**	**4.95**

Fig 3. Profile of a group 1 patient.

Group 2 Example:

20 y/o female patient presenting with severe poorly controlled seizures and focal neurological deficits.

The patient received combination treatment that included embolization, surgery and radiation therapy.

Right posterior frontal AVM supplied predominantly by right middle cerebral artery branches (Spetzler-Martin III).

The flow features in this patient are summarized below.

Artery	WSS (F) N/m^2	Flow (ml/sec)	Velocity (cm/s)	Diameter (mm)
RICA	**1.952**	**5.69**	**43.9**	4.27
LICA	1.15	4.19	39.3	3.93
RMCA	**2.252**	**5.09**	**41.9**	3.96
LMCA	1.134	3.19	29.8	3.75
Main Feeder	1.095	1.56	23.3	2.96

Fig 5. Profile of a group 2 patient.

An example of a group 2 patient is presented in Figs 5 and 6. Fig 5 summarizes this patient, who had a right frontoparietal AVM fed from the anterior circulation, and had focal neurologic deficits as well as severe headaches/seizures. Fig 5 shows hemodynamic data from this patient, showing similar vessel caliber but increased WSS, flow, and velocity. Fig 6*A* shows a maximum intensity projection of a complex difference image acquired using PC-VIPR to establish the orientation of the AVM, and Fig 6*B* shows a velocity image of the whole brain. Note similar diameter of the ICA/MCA of the right (ipsilateral to AVM) compared with the left side. Fig 6*C* shows a WSS map of the whole brain, while Fig 6*D* shows a detailed WSS map of the circle of Willis; note increased WSS in the MCA and ICA of right-sided vessels compared with the left side.

Discussion

Our pilot clinical study examined 10 patients with AVMs. The group 1 patients ($n = 4$) presented either with no symptoms (AVM discovered as an incidental finding) or mild, stable symptoms amenable to medical management. The group 2

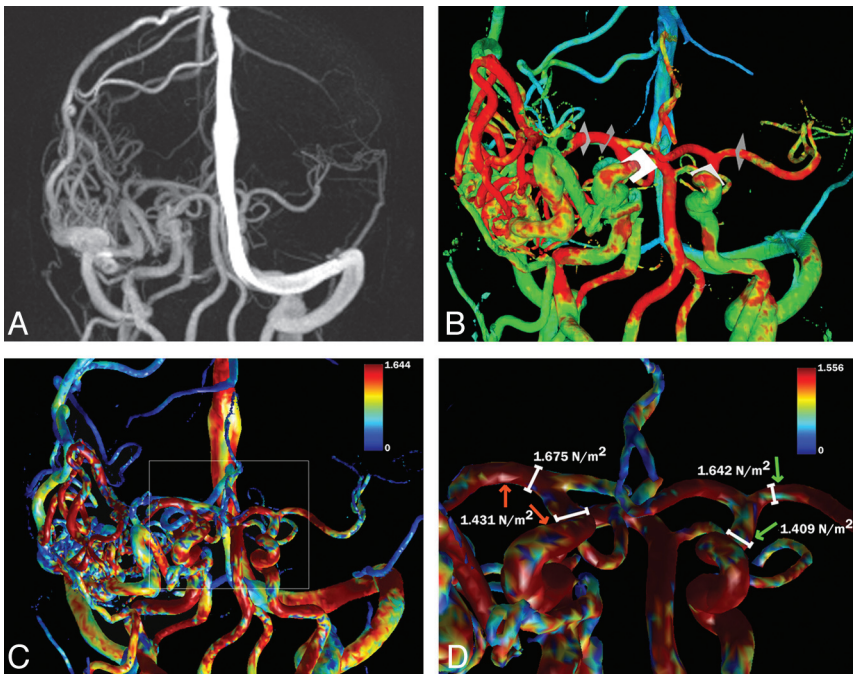

Fig 4. *A*, Maximum intensity projection of a complex difference image acquired using PC-VIPR, showing a right temporal AVM. *B*, Velocity image of the right temporal AVM, showing cut-planes being made in arterial feeders and normal contralateral vessels. *C*, WSS map of the whole brain, showing similar WSS but increased diameter in feeding vessels compared with normal contralateral vessels. *D*, Detail WSS map showing the circle of Willis and WSS measurements in feeding vessels; note similar WSS values in feeders compared with contralateral normal vessels.

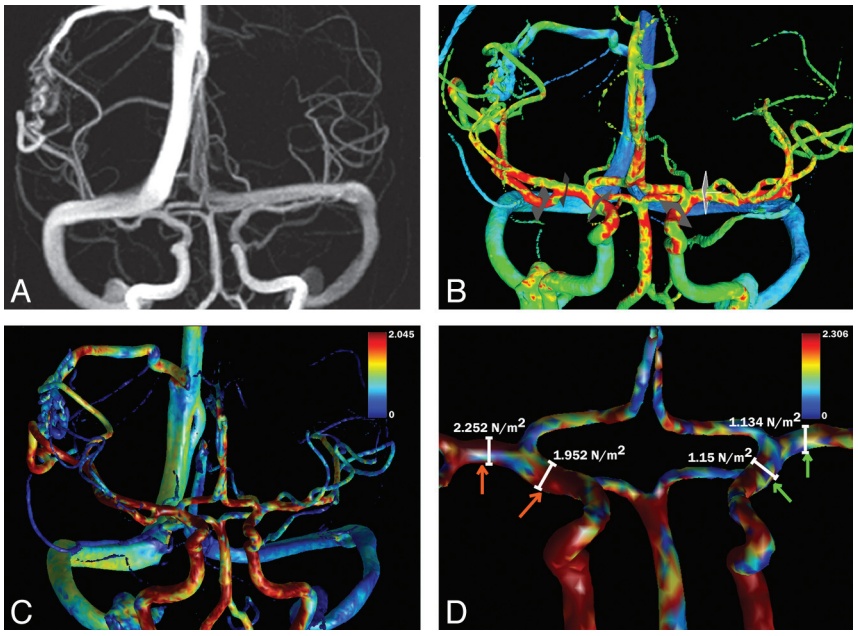

Fig 6. *A*, Coronal maximum intensity projection of a complex difference image acquired using PC-VIPR, showing a right frontoparietal AVM. *B*, Velocity image of the right frontoparietal AVM, showing cut-planes being made in arterial feeders and normal contralateral vessels. *C*, WSS map of the whole brain, showing similar diameter but increased WSS in feeding vessels compared with normal contralateral vessels. *D*, Detail WSS map showing the circle of Willis and WSS measurements in feeding vessels; note increased WSS values in feeding arteries (*red arrows*) compared with contralateral normal vessels (*green arrows*).

patients ($n = 6$) received treatment after presenting symptomatically with hemorrhage, neurologic deficits, or severe headaches/seizures. Both groups had increased flow in vessels feeding the AVM compared with normal contralateral vessels, and this difference was statistically significant. This is expected, as AVMs are generally high-flow environments, because of the lack of a resistive capillary system. Both groups had larger diameter in feeding vessels compared with normal contralateral vessels, but the difference was only statistically significant in group 1 patients. We found no statistical difference between WSS in vessels feeding AVMs compared with normal contralateral vessels in group 1, while group 2 had higher WSS in feeding vessels than normal contralateral vessels, and this difference was statistically significant.

The differences in hemodynamics in the 2 groups may have clinical significance, because group 2 patients, who presented with severe symptoms, focal neurologic deficits, or ICH, had higher levels of WSS in feeding vessels compared with normal contralateral vessels. They also exhibited less arterial dilation than group 1 patients. Higher WSS in feeding vessels in these patients may put them at higher risk of hemorrhage, as compensatory dilation of the feeding vessels normalizing shear stress and circumferential strain may not yet be completed. We believe that, when combined with existing methods of risk evaluation, hemodynamic analysis has clinical potential in improving the identification of patients at higher risk of intracranial hemorrhage.

Given the high lifetime risk of rupture, prompt treatment is considered the standard of care for younger individuals with AVMs, whether or not they present with symptoms. The Spetzler-Martin grading scale[20] uses AVM size, presence of deep venous drainage, and eloquence of adjoining areas to define AVM grade, and it is widely used as the standard for assessment of surgical risk. Other assessments proposed in recent years take into account additional factors such as age, unruptured presentation, compact or diffuse morphology, and deep brain location.[21] AVMs are typically treated with radiosurgery, embolization, or resection, or a combination of these techniques. Radiosurgery uses high doses of radiation to treat AVMs and carries a 12%–34% complication rate, with a 20% rate of permanent complications in several series.[22,23] Embolization carries up to a 20% complication rate with 7.5%–11% permanent neurologic morbidity[24-26] and often requires multiple treatments. Surgery carries an 18%–41% chance of complications, with 15% of patients experiencing disabling deficits and 3.6% incidence of mortality in some series.[27,28]

While the standard of care for patients presenting with signs of hemorrhage and significant risk factors is timely treatment, there is less consensus on the best course of action for asymptomatic patients with unruptured AVMs. A retrospective study from Scotland[29] identified a higher hazard ratio in the intervention group compared with the group that was conservatively managed with supportive care only. These findings and others have prompted large-scale prospective trials such as the ARUBA trial.[30,31] Given the uncertain outcomes in evaluating asymptomatic patients without significant risk factors, a better understanding of which AVMs carry an increased risk of hemorrhage may help identify patients who would benefit from definitive treatment and those in whom observation is an acceptable alternative.

In a study conducted using Doppler sonography, Rosseti and Svendsen found that arterial feeders to AVMs have similar WSS compared with normal contralateral arteries, despite having larger diameters and velocities.[32] They hypothesized that the increase in vessel caliber was secondary to increased WSS stimulating vessel dilation, which normalizes WSS. Therefore, patients in whom WSS is similar in AVM feeders,

compared with normal contralateral vessels, may have already compensated for high feeder WSS, while patients who have a differential between feeders and contralateral vessels may not yet have completed compensatory changes, and their vessels may be subject to higher strain. Therefore, analysis of hemodynamic parameters such as WSS may have promise in stratifying patients, by defining the regional hemodynamic conditions associated with the AVM.

Several techniques are currently used in the assessment of intracranial WSS. While there is no reference standard for WSS measurement, computer simulations using CFD are considered the best method currently available for the estimation of WSS in the neurovasculature.[33] However, the use of CFD in arteriovenous malformations is very problematic, due to the propensity of AVMs to recruit arterial feeders from numerous arterial territories, and their complicated venous drainage pattern and geometry, which makes assumptions about boundary conditions and inputs/outputs very challenging. Intracranial sonography is also used for WSS calculations, but the sonic properties of the cranial vault allow a limited field of view, and sonography measurements are also very operator dependent.

Highly accelerated PC-VIPR has the advantage of direct in vivo measurements of velocity from the phase-contrast component and markedly faster scan times, with higher spatial resolution compared with other 4D techniques.[27,31] PC-VIPR also captures a 220-mm field of view, which includes the entire brain and the carotid and vertebral systems, and can evaluate both arterial supply and venous drainage of AVMs. This is a significant advantage compared with other angiographic techniques, especially when imaging arteriovenous malformations, which can be very large in size. Velocity measurements from PC-VIPR have been validated by comparison with reference standards such as sonography and 2D PC-MRA. WSS calculations and calculations of derivatives such as velocity and streamlines have demonstrated clinical value in assessing areas of complex flow.[34-37] Hemodynamic values measured using endovascular catheters in animal models have shown a strong correlation with values acquired using PC-VIPR.[37-39] The WSS computational model used in this study has also been previously validated.[27] We feel that, despite the challenges inherent in the assessment of hemodynamics of AVMs, including complicated geometry, large size, and necessity of high spatial resolution, PC-VIPR is an effective technique in the assessment of these complicated neurovascular lesions.

A significant limitation of this report is that true WSS is impossible to measure in vivo. WSS values reported in this study are only estimates. Compared with CFD or sonography, phase-contrast techniques such as PC-VIPR have limitations in assessment of velocity at the boundary zone near the vessel wall due to lower spatial resolution. However, creating flow models of AVMs is problematic for CFD due to the complex vascular morphology and geometry. Transcranial Doppler Ultrasound is not well suited for AVM flow analysis because of the limited number of vessels that can be reliably imaged through the temporal acoustic window. Thus, PC-VIPR represents a good option for assessing both the anatomy and hemodynamics of AVMs due to adequate spatial resolution, fast scan time, acquisition of velocity information, and large field of view. One further limitation of this study is that both the hemodynamic data and clinical picture of patients in our studies represent the clinical presentation and flow conditions at only 1 point in time. Long-term study of hemodynamics in this patient group will be necessary to determine the efficacy of hemodynamic analysis in risk stratification. However, we believe the data presented in this report illustrate the promise of hemodynamic analysis in the evaluation of this patient population. We intend to combine hemodynamic analyses with existing risk-factor analysis techniques to create a multivariate model that may offer an improvement in risk stratification.

Conclusions

AVMs present a clinical challenge to clinicians because of their high lifetime risk of hemorrhage and concomitant risks of morbidity and mortality from current treatment options. Stratifying patients into different risk categories may help prioritize treatment for patients who are at highest risk of hemorrhage. WSS is a parameter that is altered in AVM patients. We demonstrate that hemodynamic features such as WSS can be estimated in patients with AVMs in a noninvasive manner and within clinically useful imaging times using accelerated phase-contrast MRA. Hemodynamic data acquired in this study appeared to relate to the clinical presentation of 2 separate groups of patients. Estimates of WSS may improve the characterization and staging of AVMs by demonstrating altered hemodynamics.

Acknowledgments

We would like to acknowledge the advice and support of Michael Markl, PhD, and Auerlein Stalder, PhD, who provided one of the software tools we used for hemodynamic analysis. In addition, we greatly appreciate the advice provided by Alex Frydrychowicz, MD, regarding intracranial hemodynamics, and the assistance of Kari Pulfer in patient recruitment.

Disclosures: Oliver Wieben—*UNRELATED: Other:* GE Healthcare,* Comments: Our institution is receiving research support from GE Healthcare. Research supported by NIH R21 EB009441, NIH RO1 HL072260. (**Money paid to institution*)

References

1. da Costa L, Wallace C, ter Brugge K, et al. **The natural history and predictive features of hemorrhage from brain arteriovenous malformations.** *Stroke*, 2009;40:100–05
2. Stapf C, Mast H, Sciacca R, et al. **Predictors of hemorrhage in patients with untreated brain arteriovenous malformation.** *Neurology* 2006;66:1350–55
3. Young WL. **Arteriovenous malformations clinical and genetic risk stratification.** Presented at the 49th Annual Meeting of the American Society of Neuroradiology, Seattle, Washington, June 6, 2011
4. Graf C, Perret G. **Bleeding from cerebral arteriovenous malformations as part of their natural history.** *J Neurosurgery* 1983;58:331–37
5. Laakso A, Dashti R, Juvela S, et al. **Risk of hemorrhage in patients with untreated Spetzler-Martin grade IV and V arteriovenous malformations: a long-term follow-up study in 63 patients.** *Neurosurgery* 2011;68:372–78; discussion 378
6. Ondra SL, Troupp H. **The natural history of symptomatic arteriovenous malformations of the brain: a 24-year follow-up assessment.** *J Neurosurg* 1990;73:387–91
7. Hashimoto T, Emala C, Joshi S, et al. **Abnormal pattern of Tie-2 and vascular endothelial growth factor receptor expression in human cerebral arteriovenous malformations.** *Neurosurgery* 2000;47:910–19
8. Kamiya A, Togawa T. **Adaptive regulation of wall shear stress to flow change in the canine carotid artery.** *Am J Physiol* 1980;239:H14–21
9. Girerd X, London G, Boutouyrie P, et al. **Remodeling of the radial artery in response to a chronic increase in shear stress.** *Hypertension* 1996;27:799–803
10. Malek A, Alper S, Izumo, S. **Hemodynamic shear stress and its role in atherosclerosis.** *JAMA* 1999;282:2035–42
11. Chen Y, Pawlikowska L, Yao J, et al. **Interleukin-6 involvement in brain arteriovenous malformations.** *Ann Neurol* 2006;59:72–80

12. Walker J, Su H, Shen F, et al. **Arteriovenous malformation in the adult mouse brain resembling the human disease.** *American Neurological Association* 2011;69:954–62
13. Corti P, Young S, Chen C, et al. **Interaction between ALK1 and blood flow in the development of arteriovenous malformations.** *Development* 2011;138: 1573–82
14. Stalder AF, Russe MF, Frydrychowicz A, et al. **Quantitative 2D and 3D phase contrast MRI: optimized analysis of blood flow and vessel wall parameters.** *Magn Reson Med* 2008;60:1218–31
15. Johnson K, Lum D, Turski P, et al. **Improved 3D phase contrast MRI with off-resonance corrected dual echo VIPR.** *Magn Reson Med* 2008;60:1329–36
16. Wu Y, Chang W, Johnson K, et al. **Fast whole brain 4D contrast enhanced MR angiography with velocity encoding using undersampled radial acquisition and highly constrained projection reconstruction (HYPRFlow): image quality assessment in volunteer subjects.** *AJNR Am J Neuroradiol* 2011;32:E47–50
17. Velikina JV, Johnson KM, Wu Y, et al. **PC HYPR flow: a technique for rapid imaging of contrast dynamics.** *J Magn Reson Imaging* 2010;31:447–56
18. Wetzel S, Meckel S, Frydrychwocz A, et al. **In vivo assessment and visualization of intracranial arterial hemodynamics with flow sensitized 4D MR imaging at 3T.** *AJNR Am J Neuoradiol* 2007;28:433–38
19. Markl M, Wegent F, Zech T, et al. **In-vivo wall shear stress distribution in the carotid artery: effect of bifurcation geometry, internal carotid stenosis, and recanalization therapy.** *Circulation* 2010;3:647–55
20. Spetzler R, Martin N. **A proposed grading system for arteriovenous malformations.** *J Neurosurg* 1986;65:476–83
21. Lawton M, Kim H, McCulloch C, et al. **A supplementary grading scale for selecting patients with brain arteriovenous malformations for surgery.** *Neurosurgery* 2010;66:702–13
22. Skjøth-Rasmussen J, Roed H, Ohlhues L, et al. **Complications following linear accelerator based stereotactic radiation for cerebral arteriovenous malformations.** *Int J Radiat Oncol Biol Phys* 2010;77:542–47
23. Buis D, Meiker O, van den Berg R, et al. **Clinical outcome after repeated radiosurgery for brain arteriovenous malformations.** *Radiother Oncol* 2010;95: 205–56
24. Weber W, Kis B, Siekmann R, et al. **Endovascular treatment of intracranial arteriovenous malformations with Onyx: technical aspects.** *AJNR Am J Neuroradiol* 2007;28:371–77
25. Taylor CL, Dutton K, Rappard G, et al. **Complications of preoperative embolization of cerebral arteriovenous malformations.** *J Neurosurg* 2004;100: 810–12
26. Starke R, Komotar R, Otten M, et al. **Adjuvant embolization with N-butyl cyanoacrylate in the treatment of cerebral arteriovenous malformations.** *Stroke* 2009;40:2783–90
27. Morgan M, Johnston I, Hallinan J, et al. **Complications of surgery for arteriovenous malformations of the brain.** *J Neurosurg* 1993;78:176–82
28. Hartmann A, Stapf C, Hofmeister C, et al. **Determinants of neurological outcome after surgery for brain arteriovenous malformation.** *Stroke* 2000;31: 2361–64
29. Wedderburn C, Beijnum J, Bhattacharya J, et al. **Outcome after interventional or conservative management of unruptured brain arteriovenous malformations: a prospective, population-based cohort study.** *Lancet* 2007;7: 223–30
30. Fiehler J, Stapf C. **ARUBA – beating natural history in unruptured brain AVMs by intervention.** *Neuroradiology* 2008;50:465–67
31. Mohr J, Moskowitz A, Stapf C, et al. **The ARUBA trial: current status, future hopes.** *Stroke* 2010;41:537–40
32. Rosseti S, Svendsen P. **Shear stress in cerebral arteries supplying arteriovenous malformations.** *Acta Neurochir (Wien)* 1995;137:138–45
33. Wood N, Weston S, Kilner P, et al. **Combined MR imaging and CFD simulation of flow in the human descending aorta.** *J Magn Reson Imaging* 2001;13:699–713
34. Chang W, Landgraf B, Kecskemeti S, et al. **Velocity measurements in the middle cerebral arteries of healthy volunteers using 3D-radial PC HYPRFlow: comparison with transcranial Doppler sonography and 2D phase-contrast MR imaging.** *AJNR Am J Neuroradiol* 2011;32:54–59
35. Jiang J, Johnson K, Valen-Sendstad K, et al. **Comparison of aneurismal hemodynamics between 4-D accelerated phase-contrast MR angiography and computational fluid dynamics simulations: initial experience in a canine aneurysm model.** Presented at the American Society of Mechanical Engineering Summer Bio-Engineering Conference, Naples, FL, June 17, 2010
36. Hope MD, Purcell DD, Hope TA, et al. **Complete intracranial arterial and venous blood flow evaluation with 4D flow MR imaging.** *AJNR Am J Neuroradiol* 2009;30:362–66
37. Gu T, Korosec F, Block W, et al. **PC VIPR: a high-speed 3D phase-contrast method for flow quantification and high-resolution angiography.** *AJNR Am J Neuroradiol* 2005;26:743–49
38. Moftakhar R, Aagaard-Kienitz B, Johnson K, et al. **Noninvasive measurement of intra-aneurysmal pressure and flow pattern using phase contrast with vastly undersampled isotropic projection imaging.** *AJNR Am J Neuroradiol* 2007;28:1710–14
39. Turk AS, Johnson KM, Lum D, et al. **Physiologic and anatomic assessment of a canine carotid artery stenosis model utilizing phase contrast with vastly undersampled isotropic projection imaging.** *AJNR Am J Neuroradiol* 2007;28: 111–15